Cooperative optical bistability in the dimer system $Cs_3Y_2Br_9$:10% Yb^{3+}

Markus P. Hehlen[a)] and Hans U. Güdel
Institut für anorganische Chemie, Universität Bern, Freiestrasse 3, 3000 Bern 9, Switzerland

Qize Shu and Stephen C. Rand
Division of Applied Physics, 1049 Randall Laboratory, University of Michigan, Ann Arbor, Michigan 48109-1120

In single crystals of the dimer compound $Cs_3Y_2Br_9$:10% Yb^{3+} below 31 K, both visible (VIS) and near-infrared (NIR) luminescence intensities were found to exhibit hysteresis as a function of incident NIR intensity and temperature. The optical bistability is intrinsic to $Cs_3Y_2Br_9$:10% Yb^{3+} and not a result of an external feedback. Lowering the temperature to 11 K strongly enhances the all-optical switching behavior. The switching on VIS cooperative upconversion and NIR luminescence transitions occurs simultaneously and with opposite polarity reflecting the competition of both emission processes. On/Off switching ratios of up to 4.8 and 1.7 were observed for VIS and NIR luminescence intensities. Using NIR luminescence spectroscopy, differences in the internal sample temperature of up to 7 K were found between the upper and lower branches of the hystereses. A two-level density-matrix model is developed which includes ground- and excited-state interactions and shows that the intrinsic bistability due to a local field different from the external field is strongly amplified by the nonlinear cooperative upconversion process. Alternatively, a rate-equation model is presented which takes the multilevel nature of the ions into account but is more phenomenological in nature. Formally, the two models are shown to be equivalent, and they qualitatively explain all major experimental observations. It is found both theoretically and experimentally that increasing the coupling within Yb^{3+} dimers and/or decreasing energy migration through the Yb^{3+} lattice enhances switching and renders it easier to observe intrinsic optical bistability. © *1996 American Institute of Physics.* [S0021-9606(96)01004-1]

I. INTRODUCTION

The consequences of cooperative interactions between transition metal and rare-earth ions in insulating crystals are manifold. For example, magnetic ordering phenomena are usually attributed to exchange or magnetic dipole–dipole interactions among the magnetic ions in their electronic ground state. Interactions between electronically excited and ground state ions can lead to excitation energy transfer, energy migration and other excitonic phenomena. However, the phenomenon of intrinsic optical bistability, i.e., the presence of two stable transmission or emission intensity values for a given input intensity outside an optical cavity, has not been reported so far for a transition metal or rare earth metal compound. We have recently found that the compound $Cs_3Y_2Br_9$:10% Yb^{3+} does exhibit such behavior, and for a certain range of the relevant parameters the luminescence from this system was found to show hysteresis[1] with the possibility of optically switching between two states. In the present paper we provide a detailed account of our experimental findings, some of which were published in an earlier letter (Ref. 1). In addition, we introduce new terms into the theory of optical interactions in dense media and demonstrate their importance by comparison with experiment.

Theoretically, intrinsic bistability in dense media was first treated by Bowden and Sung.[2] In Refs. 3–6 the theory

was further developed. It was shown that ground-state, near dipole–dipole (NDD) interactions responsible for making the local or Lorentz field different from the incident field could cause optical switching. To our knowledge there have been no experimental observations of optical bistability based on such interactions so far. Our experiments on the Yb^{3+} system suggested that interactions among excited states, which had so far not been considered theoretically, might be important. A new term taking explicit account of the cooperative interaction between excited electronic states was therefore introduced in Ref. 1. The consequences of this term, together with related dephasing interactions not considered in Ref. 1, are developed in detail in terms of a density matrix model in Sec. III A of the present paper. In parallel, a rate equation model for reproducing the excited state dynamics in $Cs_3Y_2Br_9$:10% Yb^{3+} is developed in Sec. III B. The two models are shown to be equivalent, both are capable of reproducing the essential features of the observed bistability and hysteresis behavior.

The chemical system used for this study belongs to a large class of compounds with the general formula $Cs_3M_2X_9$ ($M=Ho^{3+}$,...,Lu^{3+},Y^{3+} when $X=Cl^-$; $M=Sm^{3+}$,...,Lu^{3+}, Y^{3+} when $X=Br^-$) containing the dimer units $M_2X_9^{3-}$. In these units two octahedra share a common face thus leading to a very short $M^{3+}-M^{3+}$ distance. In $Yb_2Br_9^{3-}$ the $Yb^{3+}-Yb^{3+}$ separation is only 3.83 Å, with implications both on the magnetic and optical properties. A large ground state splitting of 3 cm^{-1} resulting from exchange interactions within the dimer units was found in $Cs_3Yb_2Br_9$.[7] Optical

excitation energy in the near infrared (NIR) is easily exchanged between the two Yb^{3+} ions, thus leading to upconversion and subsequent green dimer luminescence.[8] This upconversion process is one of the keys to understanding the bistability phenomena reported here. Another key process in $Cs_3Y_2Br_9$:10% Yb^{3+} is efficient energy migration among the Yb^{3+} sites after NIR excitation. This is the result of relatively short Yb^{3+}–Yb^{3+} distances in the range of 5.8 to 8.2 Å between Yb^{3+} ions in neighboring dimers in the lattice.

We believe the implications of our results are not limited to rare earth and transition metal ions, or to the host crystal used in this work, or indeed even to solids. Our observations and theory should be relevant to a variety of other physical situations such as quasiresonant collisional interactions in dense atomic vapors[9–11] or avalanche upconversion systems.[12] A useful objective of additional observations of bistability in such systems would be improved understanding of the time dependence of the phenomenon.

II. EXPERIMENT

Single crystals of $Cs_3Y_2Br_9$:10% Yb^{3+} were grown using the Bridgman technique.[8] Optical quality samples of randomly oriented crystals were prepared following the procedures described in Ref. 13. Sample temperatures in the range of 11 to 31 K were achieved using a liquid-helium cryostat (Oxford Instruments MD4).

Near-infrared (NIR) and visible (VIS) luminescence measurements were performed using an argon-ion laser (Spectra Physics 2045) pumped Ti:sapphire laser (Schwartz Electrooptics) in standing-wave configuration. The laser output was unpolarized and typically 300 mW, TEM_{00}. A laser linewidth of about 2 GHz was achieved using an intracavity etalon. The Ti:sapphire laser intensity was controlled using a stepper-motor driven variable neutral-density filter (Balzers) and measured using a photodiode (HP 5082-4420). The laser beam was focused on the crystal ($f=150$ mm), and coaxially NIR sample luminescence was collected ($f=65$ mm). It was dispersed by a 0.85 m double monochromator (Spex 1402) using 500 nm blazed 1200 grooves/mm gratings and detected by a liquid-nitrogen cooled germanium detector (Applied Detector Corporation 403L) and a lock-in amplifier (Stanford Research SR510). In combination with two filters (KG3 and Balzers Dichrolight C54) VIS sample luminescence was detected by an S5 side-window photomultiplier (EMI 9781A) and a pico–ampere meter (Keithley 417). Laser power, VIS and NIR sample luminescence were simultaneously recorded by means of a computer-controlled 3-channel measurement.

III. THEORY

Earlier theoretical research[2–6] predicted that ground state, near dipole–dipole (NDD) interactions in dense systems not only cause the local field to differ from the incident field as pointed out by Lorentz[14] but can also cause all-optical switching. Here, we explore the important role which can be played by dipolar interactions among *excited states* in enhancing such nonlinear dynamics.
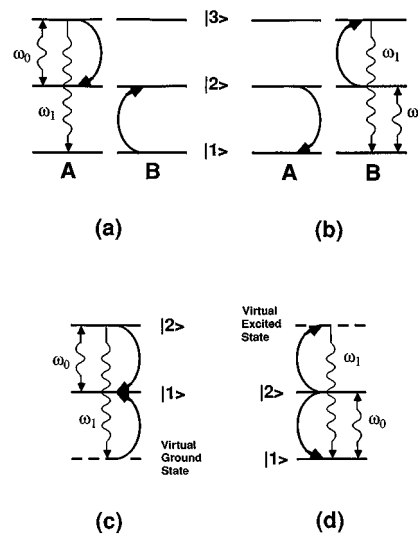

FIG. 1. Cooperative dynamics involving two 3-level atoms, giving rise to (a) cross relaxation, and (b) pair upconversion. The cooperative dynamics depicted in (a) and (b) can be described by the 2-level theoretical models (c) and (d), respectively, in which the third (intermediate) states are treated as virtual states. Wiggly arrows indicate photons, curved arrows indicate (non-radiative) cooperative relaxation processes.

First, the two-level density matrix model is extended to incorporate previously omitted excited state contributions, and intrinsic bistability dependent on a combination of ground and excited state couplings of the atoms is predicted. Quasiresonant excited state interactions are thereby shown to amplify the intrinsic nonlinear response of dense systems caused by NDD interactions. Second, an alternative rate equation treatment is introduced and compared with the density matrix approach. The rate equation model is more phenomenological in nature and has more arbitrary parameters. Nevertheless, it improves agreement with observed intensity and temperature dependences of cooperative emission. It permits the multilevel nature of the real atoms to be taken into account without considering system coherences by introducing a temperature field variable to replace the optical polarization responsible for coupling dynamic variables in the density matrix approach.

A. Density matrix approach

The excited-state energy exchange interactions of interest in this work are of two general types, as depicted in Figs. 1(a) and 1(b). In Fig. 1(a) for example, an atom *A* prepared in the upper state can relax nonradiatively to a lower level through a quasiresonant electromagnetic or spin interaction with a ground state atom *B* which undergoes a simultaneous, energy-conserving dipole transition upward. Such a process is generally referred to as cross relaxation. Excitation energy is partitioned between the excited atom and a ground state partner at a rate which is bilinear in their respective densities, and therefore *nonlinear* with respect to occupation probabilities. The reverse process, sketched in Fig. 1(b) and called cooperative upconversion, can also occur and is the process responsible for the experimental results reported here.

The dynamics of interest [Fig. 1(b)] can be treated with a two-level pair model of cooperative processes [Fig. 1(d)] derived from the Schrödinger equation. It incorporates ground state dipolar interactions through local field corrections in the optical polarization, following previous work.[5,15] However, in addition it includes excited state interactions. Of the three states shown in Figs. 1(a) and 1(b), we note that one participates merely as an intermediate state. Consequently, it can be neglected in a closed system, as illustrated in the two-level models of Figs. 1(c) and 1(d), provided that corresponding relaxation terms are incorporated into the equations of motion.

Consider first a two-level atom which interacts with light. Its lower and upper levels will be designated by $|1\rangle$ and $|2\rangle$, respectively. Its Hamiltonian

$$\hat{H} = \hat{H}_0 + \hat{H}_I \tag{1}$$

contains the isolated atom part $\hat{H}_0 = H_{22}|2\rangle\langle 2| - H_{11}|1\rangle\langle 1|$ and the optical interaction $\hat{H}_I = -\mu E_L(|2\rangle\langle 2| + |1\rangle\langle 1|)$, where H_{ii} is the energy eigenvalue of state $|i\rangle$, and μ and E_L denote the dipole matrix element and the local field, respectively. The Schrödinger equation of motion for the density matrix including relaxation terms is

$$i\hbar\dot{\rho} = [\hat{H}, \rho] + \text{relaxation terms.} \tag{2}$$

The overdot indicates a derivative with respect to time. Initially we assume the relaxation terms include only spontaneous decay and dephasing. The individual elements of the density matrix for a closed system ($\rho_{11} + \rho_{22} = 1$) yield

$$\dot{\rho}_{11} = \frac{-i\mu E_L}{\hbar}(\rho_{12} - \rho_{21}) + \gamma_2\rho_{22}, \tag{3}$$

$$\dot{\rho}_{22} = \frac{i\mu E_L}{\hbar}(\rho_{12} - \rho_{21}) - \gamma_2\rho_{22}, \tag{4}$$

$$\dot{\rho}_{21} = -i\omega_0\rho_{21} + \frac{i\mu E_L}{\hbar}(\rho_{11} - \rho_{22}) - \Gamma_{21}\rho_{21}, \tag{5}$$

$$\rho_{12} = (\rho_{21})^*. \tag{6}$$

Similar equations were considered previously in the context of dense systems by Dowling and Bowden,[16] who reduced them to the form of optical Bloch equations.[15] Following these authors we make use of a change of variables to introduce the generalized inversion $\sigma_3 \equiv \rho_{22} - \rho_{11}$ and the polarization $\sigma_{21} \equiv \tilde{\rho}_{21}$, where the tilde identifies the slowly varying part of the off-diagonal element $\rho_{21} = \tilde{\rho}_{21}\exp[-i(\omega t - kz)]$. The optical field has been taken to be

$$E_L = \tfrac{1}{2}[\mathscr{E}_L e^{-i(\omega t - kz)} + \mathscr{E}_L^* e^{i(\omega t - kz)}]. \tag{7}$$

The dephasing rate constant is $\Gamma_{21} = \tfrac{1}{2}\gamma_2 + \Gamma_{\text{ph}}$.[17] Γ_{ph} is the dephasing rate due to phonon interactions and other single-atom interactions.

The local or Lorentz field $\mathscr{E}_L$ takes ground state NDD interactions into account in dense media through the following relation for the slowly varying amplitudes of the fields:

$$\mathscr{E}_L = \mathscr{E} + \left(\frac{1}{3\epsilon_0} + s\right)P. \tag{8}$$

The fields in Eq. (8) are the microscopic electric field $\mathscr{E}_L$, the macroscopic electric field $\mathscr{E}$, and the polarization P; s is a factor (equal to 0 in cubic solids) determined by a lattice sum[18] and ϵ_0 is the permittivity of vacuum. In the rotating-wave approximation, the dynamical equations become

$$\dot{\sigma}_3 = -\gamma_2(\sigma_3 - \sigma_3^{(0)}) - i\Omega(\sigma_{21} - \sigma_{21}^*), \tag{9}$$

$$\dot{\sigma}_{21} = -i(\Delta + \epsilon\sigma_3)\sigma_{21} - \tfrac{1}{2}i\Omega\sigma_3 - \Gamma_{21}\sigma_{21}, \tag{10}$$

where the on-resonance Rabi frequency is $\Omega \equiv \mu\mathscr{E}/\hbar$. The superscript zero denotes equilibrium values which obtain in the absence of optical fields. The local field correction term is $\epsilon = n\mu^2/3\hbar\epsilon_0$, and has units of frequency since the density matrix elements are dimensionless. n is the number density and μ is the dipole transition moment. The detuning of light from the resonance frequency at ω_0 is $\Delta = \omega_0 - \omega$.

To this point, only spontaneous decay, dephasing and ground state NDD interactions have been included in the formalism. Excited state interactions of the type depicted in Figs. 1(a) and 1(b) can be accounted for with additional relaxation terms however. From basic scattering concepts, it is apparent that in the perturbative limit in which ground and excited state occupation probabilities may be considered independent, the cross-section per atom for a binary (cooperative) event with other impurity atoms is proportional to the density of the "other" species with which it can interact. Making the (usual) assumption that rapid energy migration renders all atoms in the interactive excited state equivalent, then the relevant density of the second species is clearly its macroscopic density. Without migration, because nearest neighbor interactions dominate cross relaxation and cooperative upconversion, the local excitation density would deplete rapidly. Hence for low excited state density and weak coupling, the total probability of cooperative processes is proportional to the product of the densities of the two species, justifying the form of phenomenological terms with which we now augment Eqs. (9) and (10).

From Fig. 1(d), cooperative upconversion can be seen to mediate decay of state $|2\rangle$ population ρ_{22} at a rate of $2\alpha\rho_{22}^2$. In this case the bilinear density dependence results in a square law dependence on the occupation of state $|2\rangle$ since both atoms are of the same species. Here, α is the conventional pair upconversion rate constant and has units of frequency, just like the local field correction ϵ. The factor of 2 counts the two excited atoms which decay for each cooperative upconversion event. To write this in terms of the inversion σ_3, we use the definition $\sigma_3 = \rho_{22} - \rho_{11}$ together with closure to obtain $\rho_{22} = (\sigma_3 + 1)/2$. Assuming there is negligible thermal occupation of the excited state ($\sigma_3^{(0)} = -1$), this then yields the relation $2\alpha\rho_{22}^2 = (\alpha/2)(\sigma_3 - \sigma_3^{(0)})^2$.

For detailed balance, a careful accounting of the emission wavelengths of emitting atoms must be made. The fraction f of excited state atoms which undergoes upconversion obviously cannot participate in radiative decay at the isolated atom resonance frequency ω_0. Hence the last term in Eq. (4)

giving the decay rate at ω_0 must be corrected from $\gamma_2 \rho_{22}$ to $\gamma_2(1-f)\rho_{22}$ in the presence of pair upconversion, where γ_2 is the radiative decay constant. Also, the decay rate for pair emission depends on pair density $f\rho_{22}$ through the radiative pair decay constant γ_3, contributing a relaxation term $\gamma_3 f \rho_{22}$. By requiring the decay terms written in terms of f (which group terms by emission frequency) to add up to $-\gamma_{\text{eff}}\rho_{22} - 2\alpha\rho_{22}^2$, a connection between f and the conventional upconversion coefficient α can be made while at the same time carefully separating the total loss rate into two parts: an emission rate reduction at ω_0 and a purely radiative decay contribution at the pair frequency. We require that

$$-\gamma_{\text{eff}}\rho_{22} - 2\alpha\rho_{22}^2 = -\gamma_2(1-f)\rho_{22} - \gamma_3 f \rho_{22}. \tag{11}$$

From Eq. (11) it is evident that $\gamma_{\text{eff}} = \gamma_2(1-f)$ and $f = 2\alpha\rho_{22}/\gamma_3$, a result used later to explain bistability in resonance fluorescence in the present experiments.

Adding the upconversion loss rate in Eq. (11) to the dynamical equations, Eq. (9) for the population inversion σ_3 yields

$$\dot{\sigma}_3 = -i\Omega(\sigma_{21} - \sigma_{21}^*) - \gamma_{\text{eff}}(\sigma_3 - \sigma_3^{(0)}) - \alpha(\sigma_3 - \sigma_3^{(0)})^2. \tag{12}$$

As the result of population losses due to cooperative upconversion, the polarization in Eq. (10) also acquires an intensity-dependent decay term equal to one half the rate of population loss per excited atom due to this process. This rate is $(2\alpha\rho_{22}^2)/2\rho_{22}$, where the factor $\frac{1}{2}$ accounts for the difference between polarization and population decay. This rate can be written in terms of the inversion as $\frac{1}{2}\alpha(\sigma_3+1)$. Additionally, resonant energy migration proceeds between excited ions and ground state neighbors. This process does not change the excited state occupation probability but randomly and rapidly modulates the resonant frequency of the atom excited at a particular time t, within a range limited by the inhomogenous width of the transition. To account quantitatively for dephasing, one generally introduces the second order correlation function of the discrete frequency jumps as follows:

$$\langle \delta\omega(t)\,\delta\omega(t')\rangle = 2\beta\delta(t-t').$$

Here, the Markoff approximation has been made, and β is the excitation migration rate constant for an incoherent hopping process. By assuming Gaussian statistics and rapid migration ($\beta \gg \Gamma_{21}$), it then follows in the usual way[17] that β itself is the optical dephasing rate constant. In combination with the α term, this yields a total dephasing rate constant of $\Gamma' = \Gamma_{21} + \alpha(\sigma_3+1)/2 + \beta$. Separating the constant dephasing contribution Γ from the portion depending on σ_3, and regrouping terms, the polarization equation can be written

$$\dot{\sigma}_{21} = -i(\Delta + \epsilon'\sigma_3)\sigma_{21} - \tfrac{1}{2}i\Omega\sigma_3 - \Gamma\sigma_{21}. \tag{13}$$

Here, $\epsilon' = \epsilon - i(\alpha/2)$ is a modified (complex) local field parameter and $\Gamma = \Gamma_{21} + \alpha/2 + \beta$. Notice that upconversion and migration both make contributions to constant dephasing, but that only α contributes to intensity-dependent dephasing and the local field.

Equations (12) and (13) are the principal results of this section, improving over earlier dynamical equations[1] through the addition of these dephasing terms. From them the population inversion σ_3 and the slowly varying envelope of the optical polarization $P = 2n\mu_{12}\sigma_{21}$ may be calculated. Under steady-state conditions, the time derivatives in Eqs. (12) and (13) equal zero. This yields

$$\sigma_{21} = \frac{-(1/2)i\Omega\sigma_3[\Gamma - i(\Delta + \epsilon'\sigma_3)]}{\Gamma^2 + (\Delta + \epsilon'\sigma_3)^2}. \tag{14}$$

By substituting Eq. (14) into Eq. (12) and rewriting γ_{eff} in terms of σ_3, we find

$$|\Omega|^2 = \frac{-[\sigma_3 - \sigma_3^{(0)}][\alpha(\gamma_3 - \gamma_2)(\sigma_3 - \sigma_3^{(0)}) + \gamma_2\gamma_3][(\Gamma')^2 + (\Delta + \epsilon\sigma_3)^2]}{\gamma_3\Gamma'\sigma_3}. \tag{15}$$

The quartic equation in Eq. (15) has solutions which are multivalued and predict intrinsic bistability in the inversion of cooperative dynamic systems. It is important to recognize that these solutions only apply if the system temperature (determined by σ_3) is in a steady-state. This makes it clear that the time scale for validity of these expressions is set by thermal diffusion rather than by relaxation times of the optical polarization itself, although the polarization is the only means by which the temperature of the system can change. When the upconversion rate constant α is zero, the coefficient of the quartic term in Eq. (15) vanishes and we recover results of Refs. 2–6 and 15. However, when both α and ϵ are not zero, the fourth order coefficient leads to modifications of the nonlinear dynamics which are the *joint* result of ground and excited state NDD interactions.

In Fig. 2, the solution of Eq. (15) for the steady state inversion σ_3 is used to plot $(\sigma_3 - \sigma_3^{(0)})^2$, a quantity proportional to the pair luminescence intensity, versus incident intensity $|\Omega|^2$ for various values of the upconversion rate constant α. The leftmost curve ($\alpha = 0$) shows that even without upconversion, weak bistability is predicted whenever the curve folds back on itself. This reproduces the basic results of Ben-Aryeh.[5] The steady-state relation between incident intensity $|\Omega|^2$ and inversion σ_3 is determined from Eq. (12) by setting the time derivative of σ_3 to zero. From the resulting expression, it can be shown that the curve no longer folds back on itself if the two points at which $d|\Omega|^2/d\sigma_3 = 0$ merge to form a saddle point. This occurs for a critical value of ϵ which, in the special case of $\gamma_2 = \Gamma_{21} = 1$ and $\alpha = \beta = \Delta = 0$, is given by
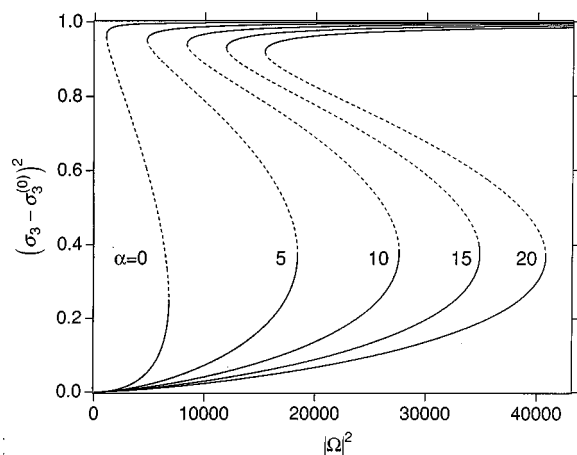
FIG. 2. Calculated [Eq. (15)] pair luminescence intensity [proportional to $(\sigma_3-\sigma_3^{(0)})^2$] versus incident intensity $|\Omega|^2$ in a system undergoing pair emission for different values of α with fixed $\beta=0$. The other parameter values are $\epsilon=100\epsilon_{cr}$, $\Delta=0$, $\Gamma'=10$, $\gamma_2=1$, $\gamma_3=4$. $\epsilon_{cr}=3\sqrt{3}$ is a critical field needed for bistability when $\alpha=\beta=0$. The solid (dashed) curves indicate stable (unstable) solutions.

FIG. 3. Calculated [Eq. (15)] pair luminescence intensity [proportional to $(\sigma_3-\sigma_3^{(0)})^2$], (a) versus incident intensity $|\Omega|^2$ for different values of β with fixed $\alpha=3.6$, and $\epsilon=100$, $\Delta=0$, $\Gamma'=4$, $\gamma_2=1$, $\gamma_3=4$, (b) versus β for different values of $|\Omega|^2$ with fixed $\alpha=3.6$, and $\epsilon=100$, $\Delta=0$, $\Gamma'=4$, $\gamma_2=1$, $\gamma_3=4$. In (a) notice that for large β switching disappears.

$$\epsilon_{cr}=3\sqrt{3}. \tag{16}$$

The solutions in the central portion of Fig. 2 between the turning points (dashed) are demonstrably unstable, causing hysteresis in the inversion versus incident intensity. As intensity is increased from zero, the predicted pair luminescence intensity at first follows the lower branch of the curve, but reaches a point at which the only stable solution available at higher powers lies on the upper branch of the curve. Here, switching to the upper branch occurs and switch down only occurs subsequently if the incident intensity falls below the point at which only a lower branch solution exists.

As the cooperative interaction rate constants α and β are increased from zero to a value comparable to ϵ, several aspects of the hysteresis change markedly. First, with $\beta=0$, a higher excitation intensity is required to reach bistability as the value of α is increased, and the hysteresis loop enlarges (Fig. 2). This is evidence that dipole–dipole interactions responsible for cooperative upconversion influence nonlinear dynamics in much the same way ground state interactions do, in keeping with the fact that both enter the coefficient of the quartic term on a similar footing, as the product $\alpha\epsilon^2$. However, the excited state dynamics depend strongly on light intensity and temperature, so that the intrinsic nonlinearity may be enhanced in a controlled fashion through the deliberate variation of these experimental parameters. If α is held fixed and β is increased, a decrease in the vertical step size of the hysteresis occurs [Fig. 3(a)]. For large enough β, hysteresis disappears altogether. In this sense it may be said that large α enhances switching, while β suppresses it.

As discussed earlier, at any given input power a portion f of the excited impurity centers undergo pair emission at a frequency $2\omega_0$. At the remaining centers, emission occurs at frequency ω_0, corresponding to the transition between levels $|2\rangle$ and $|1\rangle$. Thus if we consider resonance fluorescence, the system emits (NIR) radiation at an intensity given by
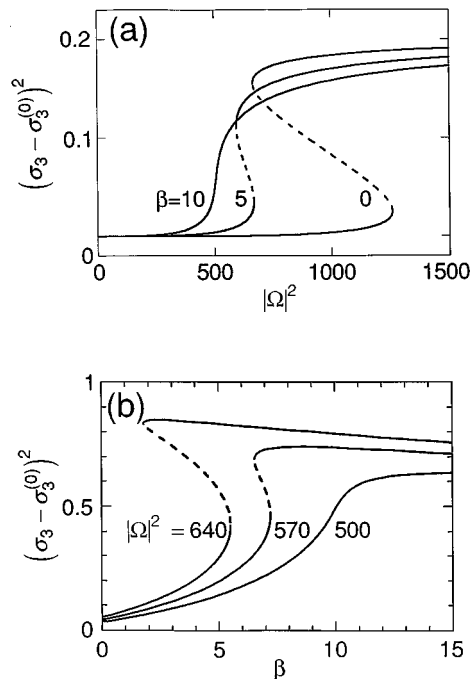
$I(\omega_0)\propto\gamma_{eff}\rho_{22}=\gamma_2\rho_{22}(1-f)$. Using the expression for f obtained from Eq. (11), this becomes $I(\omega_0)\propto[\gamma_2\rho_{22}-2\alpha\gamma_2\rho_{22}^2/\gamma_3]$. Thus the resonance fluorescence intensity should vary as

$$I(\omega_0)\propto\gamma_2\left[(\sigma_3-\sigma_3^{(0)})-\frac{\alpha}{\gamma_3}(\sigma_3-\sigma_3^{(0)})^2\right]. \tag{17}$$

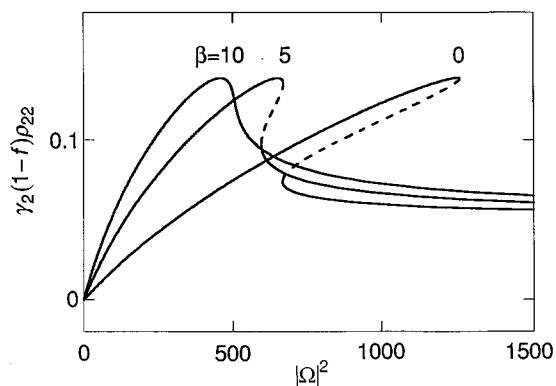The resulting behavior is illustrated in Fig. 4. As incident

FIG. 4. Predicted [Eqs. (15) and (16)] (near-infrared) resonance luminescence intensity [proportional to $\gamma_2(1-f)\rho_{22}$] versus incident intensity $|\Omega|^2$ in a system undergoing (visible) cooperative pair emission. The calculation of the luminescence intensity is described in Sec. III A and for small values of β it exhibits a switching polarity opposite to that in Figs. 2 and 3. For large β switching disappears. The parameter values are $\alpha=3.6$, $\epsilon=100$, $\Delta=0$, $\Gamma'=4$, $\gamma_2=1$, $\gamma_3=4$. The solid (dashed) curves indicate stable (unstable) solutions.

intensity is increased, resonance fluorescence intensity should at first increase by following the upper branch of the curve, but then suddenly *drop* to a lower (nearly constant) stable branch above a critical intensity. For different α/γ_3 ratios, other interesting variants of the curve are predicted. For example, the stable branches cross in a bowtie fashion for small α; for large enough α, the lower stable branch is zero for all intensities above the critical value corresponding to Eq. (18). The main result of Eq. (17), however, is that bistable switching on singly (Fig. 4) and doubly (Figs. 2 and 3) excited pair emission transitions should have opposite polarity.

An interesting consequence of this analysis obtained directly from the relation $I(\omega_0) \propto \gamma_2 \rho_{22} (1-f)$ is that resonance fluorescence is expected to *vanish* if $f=1$. This phenomenon occurs at a critical excited state density, which is

$$(\rho_{22})_{cr} = \frac{\gamma_3}{2\alpha}. \tag{18}$$

Notice that if $\gamma_3 > \alpha$, then resonance fluorescence can never be completely extinguished by the pair process, since the maximum attainable value of ρ_{22} is $\frac{1}{2}$. However, if $\alpha > \gamma_3$ then at some *finite* level of steady-state excitation, all radiation from the sample would consist of cooperative upconversion.

While the results above are most pertinent to stationary atoms in solids, they have much broader implications. For example, the absorption behavior of ultracold colliding atoms with nearly identical ground and excited state transition energies can also be expected to exhibit hysteresis on selected transitions at high densities, since absorption is proportional to $-\sigma_3$. At microkelvin temperatures and below, atoms are essentially at rest on the time scale of excited state relaxation. That is, internuclear separation does not change appreciably during the spontaneous emission lifetime. Consequently, behavior related to that calculated here for stationary atoms in a concentrated rare earth solid should be observable in dense, ultracold gases too. This implies it would be worthwhile to incorporate these quasiresonant interactions in new extensions of theories of the local field[18] in dense atomic systems.

B. Rate equation approach

Although rate equations describing population dynamics explicitly omit the coherent polarizations developed within optical media, they can often account for coherence-related phenomena by the introduction of extra degrees of freedom through additional variables. Rate equations also make it easier to describe multilevel systems by decreasing the number of coupling terms between equations. In this section we therefore examine a three-level rate equation model as an alternative to the density matrix approach. We find that indeed it is possible to predict the same switching behavior described above by introducing temperature as a crucial independent degree of freedom which implicitly couples the coefficient for migration nonlinearly to populations in an Yb^{3+} dimer system.
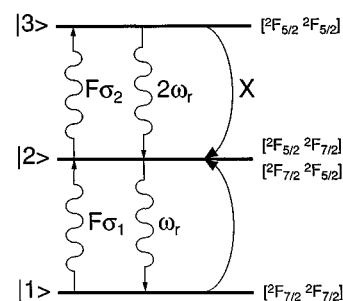

FIG. 5. Schematic representation of the ground $[^2F_{7/2}, ^2F_{7/2}]$, singly $[^2F_{7/2}, ^2F_{5/2}]$ and doubly $[^2F_{5/2}, ^2F_{5/2}]$ excited states of an $[Yb_2Br_9]^{3-}$ dimer in $Cs_3Y_2Br_9$:Yb^{3+}. Wiggly arrows indicate photons. Curved arrows indicate (nonradiative) energy-transfer processes.

As in the previous section, we assume that cooperative transitions occur at Yb^{3+} dimers in which the individual ions have only a $^2F_{7/2}$ multiplet ground state and a $^2F_{5/2}$ multiplet excited state. Thus the dimer states consist of a ground state $[^2F_{7/2}, ^2F_{7/2}]$, a singly excited state $[^2F_{7/2}, ^2F_{5/2}]$, and a doubly excited state $[^2F_{5/2}, ^2F_{5/2}]$. However, unlike the previous density matrix calculation, we work in a pair basis which makes it possible to incorporate spatial energy migration as a *population decay term* instead of a dephasing term.

Neglecting crystal field splittings, the dimer is treated as a three-level system and the above three states are labeled $|1\rangle$, $|2\rangle$, and $|3\rangle$, respectively. The possible dimer transitions are illustrated in Fig. 5, and may be described by the following nonlinear, coupled differential equations:

$$\dot{N}_1 = -F\sigma_1 N_1 + \omega_r N_2 - X N_1 N_3, \tag{19}$$

$$\dot{N}_2 = F\sigma_1 N_1 - F\sigma_2 N_2 - \omega_r N_2 + 2\omega_r N_3 + 2X N_1 N_3, \tag{20}$$

$$\dot{N}_3 = F\sigma_2 N_2 - 2\omega_r N_3 - X N_1 N_3. \tag{21}$$

In Eqs. (19)–(21), F is the photon density, σ_i are absorption cross sections, ω_r is the radiative decay constant and X is the rate constant for cross relaxation of two dimers. The overdots indicate a derivative with respect to time. Note that the radiative decay constants for states $|3\rangle$ and $|2\rangle$ differ by a factor of 2 because of twofold degeneracy of the singly excited dimer state $|2\rangle$. The radiative relaxation pathway $|3\rangle \rightarrow |1\rangle$ has been neglected due to the very low oscillator strength of this transition.[8] This model is formally analogous to that used to analyze the excited-state dynamics in the avalanche system Ni^{2+}-doped $CsCdCl_3$.[19] This similarity is reflected in the symmetry evident in Figs. 1(a) and 1(b) between avalanche and cooperative upconversion models. The dimer cross relaxation rate $X N_1 N_3$ introduces resonant energy migration in the same fashion as Ni,[20] who also used a pair basis of states. This process is sketched in Fig. 6.

In the steady-state limit, the solution of Eqs. (19)–(21) yields a quadratic equation with only a single, stable solution for N_3. The population can be a steep function of incident laser power, but does not develop a discontinuity. Taking crystal-field splittings into account in both the excited and ground state manifolds requires phonon emission, as shown in Fig. 7. Consequently, if an avalanche condition were to

FIG. 6. Schematic representation of the cross relaxation X of two $[Yb_2Br_9]^{3-}$ dimers. The asterisks indicate Yb^{3+} ions in the $^2F_{5/2}$ excited state.

occur, absorption would be high and the internal temperature of the illuminated region would exceed that of the surrounding medium. The energy transfer rate constant X would develop a temperature dependence because it depends on spectral overlap between donor emission and acceptor absorption[21] which changes as the thermal distribution of ions among the Stark levels changes. Although no experimental information is currently available regarding the dependence of internal temperature T_i on incident power F, or energy transfer rate constant X on internal temperature T_i, we simulated the behavior of the Yb^{3+} system on the basis of several reasonable assumptions.

First, the internal temperature T_i was assumed to depend linearly on the rate of phonon energy emission or phonon power P_{ph}[22]

$$T_i = T_0 + \eta P_{ph}. \tag{22}$$

Here, T_0 is the external sample temperature and η is a constant characteristic of the host lattice. During the excitation steps $|1\rangle \rightarrow |2\rangle$ and $|2\rangle \rightarrow |3\rangle$ (see Fig. 5), phonons of energy $h\nu_1$ are created at a rate $F\sigma_1 N_1$ and $F\sigma_2 N_2$, respectively. During relaxation, phonons with energies $h\nu_2$ and $h\nu_3$ are created for both steps $|3\rangle \rightarrow |2\rangle$ and $|2\rangle \rightarrow |1\rangle$ at rates of $2\omega_r N_3$ and $\omega_r N_2$, respectively. If we assume for simplicity that branching ratios of radiative transitions from the emitting state to all final states are equal, then the emitted phonon power is

$$P_{ph} = Fh\nu_1(\sigma_1 N_1 + \sigma_2 N_2)$$
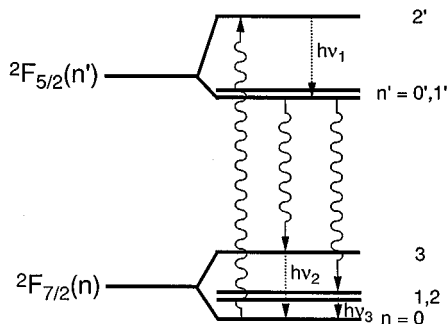$$+ \omega_r(2N_3 + N_2)(\tfrac{1}{4}h\nu_2 + \tfrac{1}{2}h\nu_3). \tag{23}$$

FIG. 7. Schematic energy-level structure of Yb^{3+} in $Cs_3Y_2Br_9$ taken from Ref. 8. The labels $n=0,1,2,3$ and $n'=0',1',2'$ denote crystal-field levels of $^2F_{7/2}$ and $^2F_{5/2}$, respectively. Wiggly arrows indicate photons. Dotted arrows indicate thermalization processes with $h\nu_1$, $h\nu_2$, and $h\nu_3$ being the energies of the emitted phonons.
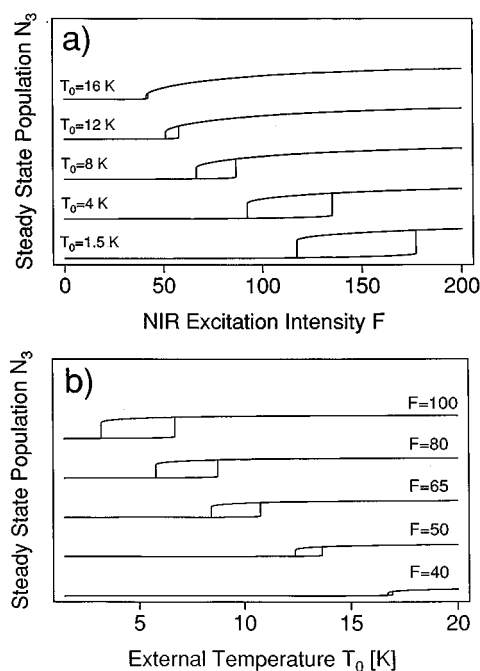

FIG. 8. Predicted [Eqs. (19)–(24)] (visible) pair luminescence intensity (proportional to the steady-state population N_3) (a) versus (near-infrared) excitation intensity F for several fixed values of the external temperature T_0, (b) versus external temperature T_0 for several fixed values of the (near-infrared) excitation intensity F. The values for the other parameters are $\sigma_1 = 0.01$, $\sigma_2 = 100$, $\omega_r = 200$ s^{-1}, $X_c = 1000$ s^{-1}, $h\nu_1 = 440$ cm^{-1}, $h\nu_2 = 120$ cm^{-1}, $h\nu_3 = 470$ cm^{-1}, $T_0 = 1.5$ K, $\eta = 1200$ K W^{-1}, $a_1 = 10$ K^{-1}, $a_2 = 2$.

Second, the interdimer energy transfer rate constant X was arbitrarily assumed to increase with increasing temperature from a low value to a high limiting value X_c (as $T_i \rightarrow \infty$)

$$X(T_i) = \tfrac{1}{2}X_c \tanh\left[\left(\frac{T_i}{a_1} + a_2\right) + 1\right]. \tag{24}$$

Here, a_1 and a_2 are parameters characteristic of donor–acceptor spectral overlap, and the form of Eq. (24) was chosen to simulate a reasonable (sigmoidal) increase of migration rate vs T. The functional dependence of X on T depends on the assumed variation of spectral overlap with temperature to be sure, but our simulations showed that virtually any increasing function of temperature guarantees hysteresis of system emission versus input power. Physically, this results from the fact that once the system reaches an avalanche condition its temperature abruptly increases, raising the value of X and lowering the avalanche threshold. When power is subsequently reduced, the reduced threshold causes the avalanche to persist to lower power levels. At low enough power it stops and X resumes its low power (low temperature) value.

Equations (19)–(24) were used to calculate the cooperative upconversion intensity as a function of both temperature and incident power. The results are shown in Figs. 8(a) and 8(b). These calculations yield results in very satisfying agreement with the experimental observations shown in the next section. With the additional parameters from the temperature dependence of X, this model develops the necessary
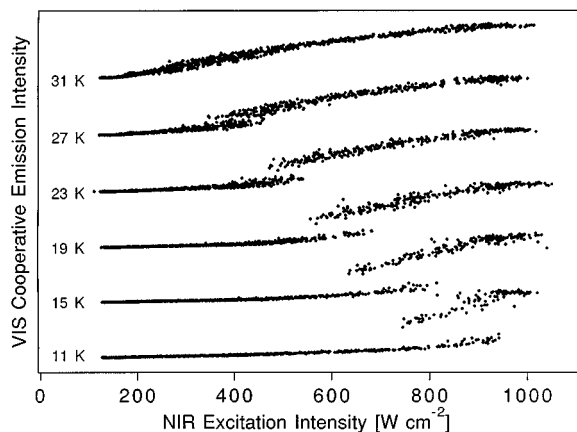
FIG. 9. Visible ($\lambda=500$ nm) cooperative emission intensity versus near infrared ($\lambda=944$ nm) excitation intensity from Yb^{3+} dimers in $Cs_3Y_2Br_9$:10% Yb^{3+} at various fixed temperatures.

FIG. 10. Visible ($\lambda=500$ nm) cooperative emission intensity versus temperature from Yb^{3+} dimers in $Cs_3Y_2Br_9$:10% Yb^{3+} at various fixed near infrared ($\lambda=944$ nm) excitation intensities.

flexibility to reproduce subtle trends in the data and is therefore useful. As with any phenomenological model however, the fundamental origin of the hysteresis remains obscure. The density matrix approach on the other hand establishes that upconversion enhances the implicit nonlinearity caused by local field corrections.[16] The migration interaction merely causes dephasing. This provides the necessary perspective on how two rather similar excited state dipole–dipole interactions can have opposite effects on the hysteresis, for in both the density matrix and the rate equation model it is found that the coupling within the ion pairs must decrease and/or the energy migration rate constant among the ions must increase with increasing temperature to account for all the observations.

Whereas the density matrix formalism provides a description of the system from first principles, the rate equation treatment is more intuitive in nature. Yet the origin of bistability is essentially the same in both: A field induces nonlinear population changes which affect the refractive index. In the density matrix approach, a local electric field correction ϵ enters the population inversion σ_3 as the product $\alpha\epsilon^2$, and in the rate equation approach a temperature field affects the population decay term $2XN_1N_3$. While superficially different, these two descriptions share the feature of index changes induced by upconversion and mediated by a field which alters level populations. Formal differences between density matrix and rate equation theory, particularly the absence of a polarization field and optical coherence in the latter, prevent any one-to-one correspondence between parameters of the two formalisms. However, an important justification for joint consideration of these equivalent theories is the perspective it provides on the nonparametric origin of cooperative bistability observed here. This mechanism permits slow, pronounced response to resonant excitation in sharp contrast to the nonresonant (parametric) phenomena in dense media considered by earlier researchers.[2–6]

IV. EXPERIMENTAL RESULTS

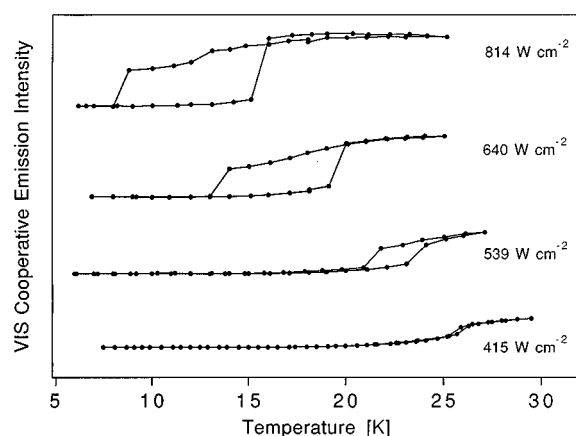Figure 9 shows the visible (VIS) cooperative lumines-

cence intensity ($\lambda=500$ nm) from $Cs_3Y_2Br_9$: 10% Yb^{3+} obtained under continuous near-infrared (NIR) laser excitation ($\lambda=944$ nm) as a function of incident laser power at several temperatures. In the temperature range shown here the power dependence of the cooperative luminescence intensity is a hysteresis. Upon increasing the laser power over a critical value an abrupt increase occurs in the luminescence intensity. Subsequent switching down only occurs when lowering the laser power well below the original switching point. Between the two discontinuities there is a bistable region where the stationary state of the system depends on its preparation. A system prepared on the upper branch of the bistable region is not able to recover from a short interruption of the excitation source and remains on the lower branch. Down along the temperature series in Fig. 9 three major effects are observed: (i) the width of the bistable region increases, (ii) the height of the discontinuities increases, and (iii) the critical incident intensity required for switching increases.

Figure 10 shows the VIS cooperative luminescence intensity from $Cs_3Y_2Br_9$: 10% Yb^{3+} obtained as a function of temperature at several fixed incident laser powers. In analogy to Fig. 9 the cooperative luminescence intensity exhibits hysteretic behavior. Up along the series of incident laser powers the same effects on the width, the height, and the critical incident intensity of the bistable region are observed as for decreasing temperature in Fig. 9.

In order to visualize the switching properties of $Cs_3Y_2Br_9$: 10% Yb^{3+} a *phase diagram of bistability* is compiled from the critical values for excitation intensity and temperature reported in Figs. 9 and 10 and presented in Fig. 11. The switching-up points (full squares) and the switching-down points (empty squares), which enclose the phase space of bistable behavior, both appear to be linearly correlated within our experimental range, the reason for this behavior being unknown at present. The intersection of the two fitted lines predicts a critical point with a maximum temperature (31.5 K) and a minimum excitation intensity (254 W cm^{-2}) for which intrinsic optical bistability in $Cs_3Y_2Br_9$: 10% Yb^{3+} occurs. As described above, lowering the temperature and/or
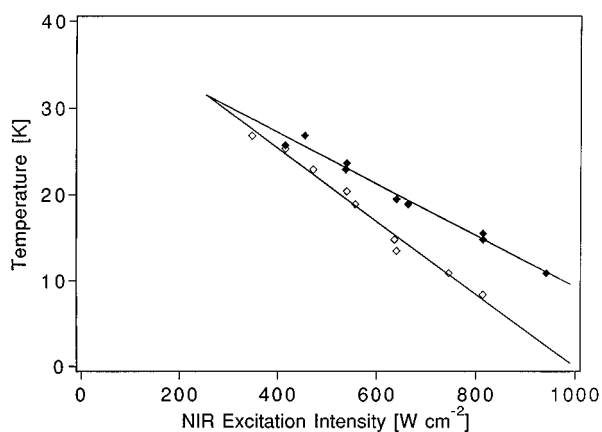
FIG. 11. Compilation of critical temperatures and near-infrared excitation intensities (taken from Figs. 9 and 10) in a phase diagram for bistability. Full (empty) squares indicate switching up (down) points of the visible cooperative emission intensity in $Cs_3Y_2Br_9$:10% Yb^{3+}. The lines are linear fits to the data points and their intersection (254 W cm^{-2}, 31.5 K) indicates a critical point for bistability to occur in this system.

increasing the laser power from this critical point widens the bistable region.

Figure 12 compares a hysteresis loop for the NIR luminescence intensity with one *simultaneously* measured for the VIS cooperative luminescence intensity as a function of incident laser power at 11 K. For these two representative curves two main features are evident: (i) NIR and VIS switching occur simultaneously and (ii) NIR and VIS hystereses have opposite polarity, i.e., an abrupt *increase* of the VIS cooperative luminescence intensity goes along with an abrupt *decrease* of the NIR luminescence intensity.

Figure 13 presents NIR luminescence spectra recorded on the upper and on the lower hysteresis branch in the bistable region. Both spectra are measured at the same temperature (11 K) and excitation intensity (830 W cm^{-2}), and they only differ in their way of preparation. Two major differences are observed: (i) the relative intensity of the two
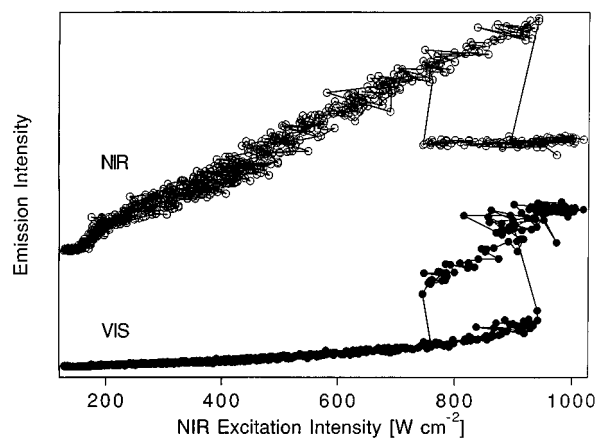

FIG. 12. Visible (λ=500 nm) cooperative luminescence intensity (full circles) and near-infrared (λ=1035 nm) luminescence intensity (empty circles) of $Cs_3Y_2Br_9$:10% Yb^{3+} measured simultaneously versus near-infrared (λ=944 nm) excitation intensity at 11 K.
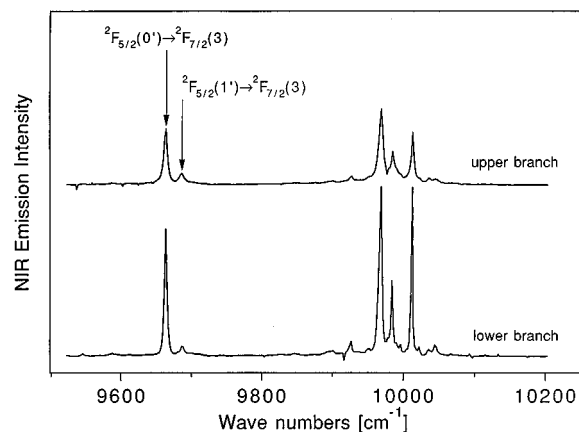

FIG. 13. Near-infrared (NIR) luminescence spectra of $Cs_3Y_2Br_9$:10% Yb^{3+} obtained using NIR (λ=944 nm) excitation. Using the same excitation intensity (830 W cm^{-2}) and temperature (11 K) the spectra are recorded on the upper and on the lower branch of the NIR intensity hysteresis shown on top of Fig. 12.

Yb^{3+} crystal-field transitions $^2F_{5/2}(1') \rightarrow {}^2F_{7/2}(3)$ and $^2F_{5/2}(0') \rightarrow {}^2F_{7/2}(3)$ increases by a factor of 2 upon switching from the lower to the upper branch, indicating a substantial increase in the internal sample temperature, and (ii) all transitions are significantly broadened in the upper-branch spectrum.

V. DISCUSSION

The spectroscopic properties of $Cs_3Y_2Br_9$: 10% Yb^{3+} reported in this paper originate from $4f$ transitions on dimers of Yb^{3+} ions.[8] Due to its very simple $4f$ energy-level structure Yb^{3+} is ideal for the detailed study of various types of $4f$ transitions as well as the coupling mechanisms within and between Yb^{3+} dimers. In the following we will first discuss the energy-level structure of Yb^{3+} in $Cs_3Y_2Br_9$ (Sec. V A) and then investigate cooperative bistability which is a result of the coupling within Yb^{3+} dimers (Secs. V B, V C, and V D).

A. Survey of Yb^{3+} transitions

Yb^{3+} has a Xe($4f$)^{13} electron configuration and only one electron is missing from the full $4f$ shell. The spin−orbit coupling splits the resulting ^2F manifold into two multiplets, a $^2F_{7/2}$ ground-state multiplet and a $^2F_{5/2}$ excited-state multiplet which has an energy of approximately 10 000 cm^{-1}. Therefore, a Yb^{3+} ion only exhibits $4f$ transitions in the near-infrared spectral region. Electrostatic interactions between Yb^{3+} and its neighboring ions in a host lattice further split both multiplets $^2F_{7/2}$ and $^2F_{5/2}$. The system studied here, $Cs_3Y_2Br_9$: 10% Yb^{3+}, is one of a family of compounds $Cs_3M_2X_9$ (M=Ho^{3+},...,Lu^{3+}, Y^{3+} when X=Cl$^-$; M=Sm^{3+},...,Lu^{3+}, Y^{3+} when X=Br$^-$) crystallizing in space group $R\bar{3}c$ with the M^{3+} ions occupying sites of approximately C_{3v} symmetry.[23] The C_{3v} crystal field lifts the J degeneracy of the M^{3+} multiplets $^{2S+1}L_J$ and gives rise to $\frac{1}{2}(2J+1)$ crystal-field levels. In the case of Yb^{3+}, the multiplets $^2F_{7/2}$ and $^2F_{5/2}$ are therefore split in 4 and 3 Kramers

doublets, respectively, which will be labeled $^2F_{7/2}(n)$ ($n=0,1,2,3$) and $^2F_{5/2}(n')$ ($n'=0',1',2'$) in the following (see Fig. 7). In a previous paper, both absorption and luminescence transitions between these crystal-field levels have been studied in detail and the crystal-field energies have been determined.[8]

In addition to the transitions on single Yb^{3+} ions described above there are cooperative transitions which arise from the coupling of two Yb^{3+} ions within a dimer. These cooperative transitions involve the simultaneous absorption or emission of radiation by two Yb^{3+} ions and thus occur around 500 nm, they have also been analyzed previously for this system.[8] In the $Cs_3M_2X_9$ lattice always two $[MX_6]^{3-}$ units share a trigonal face to form a rare earth dimer unit $[M_2X_9]^{3-}$ with a trigonal dimer axis coinciding with the trigonal crystal axis.[23] This close face-sharing arrangement leads to a M^{3+}–M^{3+} distance which is much shorter than in most compounds,[24] including the $YbPO_4$ crystal in which Yb^{3+} cooperative luminescence was observed originally.[25] Since the coupling between the lanthanide ions depends strongly on ion separation, the dimer material reported here exhibits relatively intense cooperative upconversion emission in the green. Other manifestations of strong ground- and excited-state interactions have been reported for this class of compounds.[8,13,26] In $Cs_3Yb_2Br_9$, for example, which has an Yb^{3+}–Yb^{3+} intradimer distance of only 3.83 Å, inelastic neutron-scattering measurements of the Yb^{3+} ground-state electronic splitting yield the value 3.0 cm^{-1}, which is exceptionally large for rare-earth ions in an insulating lattice.[7]

As shown in Fig. 5, the $[Yb_2Br_9]^{3-}$ dimers studied here consist of a ground state $[^2F_{7/2}(n),^2F_{7/2}(n)]$, a doubly degenerate singly excited state $[^2F_{7/2}(n),^2F_{5/2}(n')]$ around 10 000 cm^{-1} in the near infrared, and a doubly excited state $[^2F_{5/2}(n'),^2F_{5/2}(n')]$ around 20 000 cm^{-1} in the green spectral region. The labels $[\frac{7}{2}]$ and $[\frac{5}{2}]$ will be used in the following as abbreviations for the crystal-field multiplets $^2F_{7/2}(n)$ and $^2F_{5/2}(n')$, respectively. The degeneracy of the singly excited state arises from the fact that either one of the two Yb^{3+} ions within the dimer can be excited. The proper dimer wave functions are given by the symmetric and antisymmetric combinations of $[\frac{7}{2},\frac{5}{2}]$ and $[\frac{5}{2},\frac{7}{2}]$. The doubly excited states $[\frac{5}{2},\frac{5}{2}]$ in the visible spectral region are spectroscopically accessible from the ground state $[\frac{7}{2},\frac{7}{2}]$ by a one-photon or a two-photon excitation process. Both types of excitation processes have previously been investigated,[8] but only the latter will be relevant to the present work. Using a low-power Ti:sapphire-laser around 944 nm for $[\frac{7}{2},\frac{7}{2}]\rightarrow[\frac{7}{2},\frac{5}{2}]$ excitation, near-infrared (NIR) $[\frac{7}{2},\frac{5}{2}]\rightarrow[\frac{7}{2},\frac{7}{2}]$ and $[\frac{5}{2},\frac{5}{2}]\rightarrow[\frac{7}{2},\frac{5}{2}]$ as well as green upconversion (VIS) $[\frac{5}{2},\frac{5}{2}]\rightarrow[\frac{7}{2},\frac{7}{2}]$ luminescence was measured to probe excited state populations. The observed dependence of luminescence intensities on laser power will in the following be compared with the theoretical results derived in Sec. III.

B. Cooperative bistability

In Secs. III A and III B the excited-state dynamics of Yb^{3+} ions in $Cs_3Y_2Br_9$: 10% Yb^{3+} was treated in a two- and a three-level model for the density-matrix and the rate-equation approach, respectively (see Figs. 1 and 5). As pointed out earlier, these two models are equivalent and only differ in their formal way of the inclusion of spatial energy migration among Yb^{3+} ions. Whereas in the density-matrix approach energy migration contributes the additional dephasing term $\beta\sigma_{21}$ to the polarization [Eq. (13)] it was accounted for by a population decay term XN_1N_3 in the rate-equation approach [Eqs. (19)–(21)] as the latter omits any coherence developed within the optical medium. We will use the three-level pair basis described in Sec. V A (see Fig. 5) for the following discussion of spectroscopic properties.

Using NIR excitation both the singly and the doubly excited dimer states are populated after a one-photon and a sequential two-photon absorption, respectively (see Fig. 5). As multiphonon relaxation processes from the excited states are completely suppressed in this low-phonon host lattice,[13] the excited dimer states relax radiatively leading to intense VIS and NIR luminescence. Since two photons are required to reach the doubly excited dimer state $[\frac{5}{2},\frac{5}{2}]$ a nonlinear dependence of both VIS and NIR luminescence intensity on NIR excitation intensity is expected. For temperatures of about 30 K and above we find the expected behavior with the VIS luminescence intensity being a nonlinear but single-valued function of the NIR excitation intensity, see top of Fig. 9. For temperatures below 30 K, however, the luminescence intensity becomes bistable and exhibits a hysteresis both as a function of NIR excitation intensity (Fig. 9) and temperature (Fig. 10).

In Sec. III it was shown that the properties of hysteretic behavior are mainly determined by two factors: the intradimer coupling between Yb^{3+} ions (parameters α and X_c in the density matrix and the rate-equation models, respectively) and the energy migration among Yb^{3+} ions (parameters β and T_0 in the density matrix and the rate-equation models, respectively). Using inelastic neutron scattering it has been shown that the intradimer coupling in $Yb_2Br_9^{3-}$ has a constant value for temperatures up to about 50 K.[7] Thus the Yb^{3+}–Yb^{3+} coupling constant can be assumed constant over the temperature range of 7 to 31 K used in the present experiments. We therefore attribute the observed temperature dependence of the hystereses (Fig. 9) to a temperature dependence of the rate constant for the energy migration among Yb^{3+} ions. For resonant energy transfer the value of this rate constant is mainly given by the spectral overlap between donor emission and acceptor absorption, both being determined by the thermal distribution among the crystal-field levels. In the case of energy transfer between identical Yb^{3+} ions the spectral overlap and thus the energy migration rate constant decrease as the temperature is lowered.

Although no experimental data on the temperature dependence of the energy migration rate constant is presently available for this system, qualitatively, decreasing the temperature along the series of hystereses in Fig. 9 corresponds to decreasing β and T_0 in the density-matrix and rate-equation approach, respectively. All the observed trends in the series of hystereses in Fig. 9: A widening of the bistable region, an increase of the step height, and an increase of the

critical excitation intensities at the switching points are qualitatively very nicely reproduced by both the density-matrix model [see Fig. 3(a)] and the rate-equation model [see Fig. 8(a)] developed in Secs. III A and III B, respectively. No attempt was made to refine the model parameters to obtain quantitative agreement with the observed behavior. Our principal aim is to demonstrate that by using "reasonable" (see Sec. III) parameters both models are capable of reproducing the bistability behavior qualitatively or even quantitatively.

A similar trend in the width, height, and critical intensity of the hystereses is obtained when monitoring the VIS up-conversion luminescence intensity as a function of temperature for fixed NIR excitation intensity, see Fig. 10. In this case, the rate constant for energy migration is indirectly varied by variation of the temperature until it reaches a critical value characteristic for the given excitation intensity. At this point switching occurs. As shown in Figs. 3(b) and 8(b), also this experiment is nicely reproduced by the models developed in Sec. III.

C. Switching polarity

The previous section discussed the switching properties of the VIS cooperative upconversion luminescence from the doubly excited Yb^{3+} dimer state $[\frac{5}{2}, \frac{5}{2}]$. In addition, this system also exhibits bistability on the (on-resonance) NIR transitions $[\frac{7}{2}, \frac{5}{2}] \rightarrow [\frac{7}{2}, \frac{7}{2}]$ and $[\frac{5}{2}, \frac{5}{2}] \rightarrow [\frac{7}{2}, \frac{5}{2}]$. On the time scale of our detection, NIR and VIS switching occur simultaneously. In addition, the same trends of the heights and widths of the VIS hystereses described in Sec. V B are also found for the NIR hystereses. However, the main difference lies in the switching polarity, which is illustrated in Fig. 12 for two representative hystereses. The switching up (down) of the VIS upconversion luminescence intensity goes along with a switching down (up) of the NIR luminescence intensity, i.e., they have opposite polarity. In Sec. III A, a careful accounting of the NIR and VIS emission rates was made. Figures 3(a) and 4 show model calculations for the VIS and NIR luminescence intensities, respectively, as a function of excitation intensity. The opposite polarity of the two predicted bistabilities is evident. It can be understood as a result of the sudden increase of the number of Yb^{3+} ions participating in VIS cooperative upconversion luminescence at the critical point which directly lowers the fraction of Yb^{3+} ions available for NIR emission and thus lowers the luminescence intensity of this transition.

D. Internal temperature

In the rate equation approach presented in Sec. III B the internal temperature T_i was assumed to differ from the external sample temperature T_0 depending on the rate of phonon emission, i.e., the excitation state of the system [see Eqs. (22) and (23)]. This internal temperature field was subsequently used to modulate the rate constant X for energy migration [see Eq. (24)] resulting in bistable behavior. As the thermal distribution among the crystal-field levels of the $^2F_{5/2}$ excited state varies with changing temperature the relative intensities of the various NIR crystal-field transitions

$^2F_{5/2}(n') \rightarrow {}^2F_{7/2}(n)$ provide information on the internal temperature T_i of the sample. Being split by 27 cm^{-1},[8] the thermal population of the two lowest crystal-field levels of the excited-state multiplet, $^2F_{5/2}(0')$ and $^2F_{5/2}(1')$, changes appreciably in the experimental temperature range of 11 to 31 K, and the intensities of luminescence transitions from these states can therefore be used as an indicator of the internal sample temperature. This is illustrated in the NIR luminescence spectra of Fig. 13. The luminescence transitions around 9700 cm^{-1} to the highest crystal-field level $^2F_{7/2}(3)$ of the ground-state multiplet can be most easily analyzed as they are well separated from other transitions. As shown in the figure, the transition $^2F_{5/2}(1') \rightarrow {}^2F_{7/2}(3)$ shows up as a "hot band" to the $^2F_{5/2}(0') \rightarrow {}^2F_{7/2}(3)$ transition. For the series of hystereses shown in Fig. 9, NIR luminescence spectra were recorded using the same excitation intensity for both the upper and the lower branch spectrum of each hysteresis (see Fig. 13). From the observed intensity ratio of the corresponding hot and cold transitions we can estimate the internal temperature as follows: The observed intensity of a transition is proportional to the population n_i of the initial state and to the oscillator strength $f_{i \rightarrow j}$ of the transition. The relative luminescence intensity R of $^2F_{5/2}(1') \rightarrow {}^2F_{7/2}(3)$ and $^2F_{5/2}(0') \rightarrow {}^2F_{7/2}(3)$ is therefore given by

$$R = \frac{n_{(1')} f_{1' \rightarrow 3}}{n_{(0')} f_{0' \rightarrow 3}}. \tag{25}$$

If we treat $^2F_{5/2}(0')$ and $^2F_{5/2}(1')$ as a closed system $(n_{(0')} + n_{(1')} = 1)$ in thermal equilibrium the population $n_{(1')}$ is given by the Boltzman distribution

$$n_{(1')} = \frac{g_{(1')} e^{-\Delta E/kT}}{g_{(0')} + g_{(1')} e^{-\Delta E/kT}}, \tag{26}$$

where $\Delta E = 27$ cm^{-1} is the separation of the two states, $g_{(0')} = g_{(1')} = 2$ is their degeneracy, and T is the temperature. Substituting Eq. (26) into Eq. (25) and solving for T we obtain

$$T = -\frac{\Delta E}{k[\ln(g_{(0')}) - \ln(g_{(1')}) - \ln(1 - n_{(1')}) + \ln(n_{(1')})]}, \tag{27}$$

where the thermal population $n_{(1')}$ can be calculated from an experimental R value according to

$$n_{(1')} = \frac{1}{1 + \dfrac{f_{1' \rightarrow 3}}{f_{0' \rightarrow 3}} \dfrac{1}{R}}. \tag{28}$$

In 5 K absorption measurements not shown here a value of 2.83 was found for the relative oscillator strength $f_{0 \rightarrow 1'}/f_{0 \rightarrow 0'}$. Assuming the same value for the ratio $f_{1' \rightarrow 3}/f_{0' \rightarrow 3}$, the upper and lower hysteresis branch NIR luminescence spectra were analyzed using Eqs. (27) and (28). Table I summarizes the results of this analysis. Due to the limited resolution of the NIR luminescence spectra the determination of the experimental R values is difficult especially at low temperatures, and therefore the internal temperatures T_i derived from these values are only able to show

TABLE I. R is the luminescence intensity ratio of the NIR transitions $^2F_{5/2}(1') \rightarrow {}^2F_{7/2}(3)$ and $^2F_{5/2}(0') \rightarrow {}^2F_{7/2}(3)$. T_i is the calculated internal temperature (see Sec. V D).

	Upper branch		Lower branch	
T_0 (K)	R	T_i	R	T_i
7			0.067	10.4
11	0.421	20.4	0.159	13.5
15	0.370	19.1	0.190	14.4
19	0.408	20.1	0.196	14.6
23	0.403	20.0	0.211	15.0
31	0.424	20.5	0.424	20.5

trends. Whereas T_i is roughly constant on the upper branch for all external sample temperatures T_0 it increases on the lower branch with increasing temperature. Additionally, the T_i values on the upper and lower branch converge to the same value around T_i=21 K. Along with the increase in the relative hot band intensity a significant thermal broadening of all the luminescence transitions is observed (see Fig. 13). This is another manifestation of the considerable difference between external (T_0) and internal (T_i) temperature on the upper branch, indicating the high absorption and emission rates on Yb^{3+} ions after switching has occurred. For a low external temperature such as T_0=11 K the difference in calculated internal temperatures on the upper and lower branches is as high as 7 K (see Table I). These results support the concept of introducing a temperature field in the rate-equation approach, and the R values in Table I provided the experimental input for the choice of the parameter values a_1 and a_2 [see Eq. (24)] for the rate equation model calculations presented in Figs. 8(a) and 8(b).

VI. CONCLUSIONS

We have shown that the spontaneous emission from Yb^{3+} ions in $Cs_3Y_2Br_9$:Yb^{3+} exhibits intrinsic bistability as a function of incident intensity and temperature. A density-matrix model in which contributions to the nonlinear polarization from ground- and excited-state interactions between Yb^{3+} ions are treated on an equal footing gives good agreement with experiment. An alternative rate-equation model is developed and compared with the density-matrix approach. Although the rate-equation model is more phenomenological in nature and has more arbitrary parameters, both approaches are shown to be equivalent. Whereas the optical polarization is responsible for the coupling of dynamical variables in the density-matrix approach it is replaced by a temperature field variable in the rate-equation approach. A detailed balance of the various emission processes explained the opposite polarity of the switching on near-infrared and visible transitions observed in the experiments. The atom–atom coupling and the spatial energy migration are found to be the two main factors determining the bistability properties. Qualitatively, this was confirmed in the presented experiments on $Cs_3Y_2Br_9$:10% Yb^{3+} which provided a variation of the energy migration rate constant at a constant Yb^{3+}–Yb^{3+} intradimer coupling. The theory predicts that increasing atom–

atom coupling and decreasing spatial energy migration should amplify switching. Both factors are currently being investigated on various compounds of the $Cs_3Y_2X_9$:Yb^{3+} (X=Cl,Br,I) system.

The mere fact that the first example of intrinsic bistability due to atom–atom interactions has emerged from a cooperative upconversion system supports the general conclusion that resonant excited-state interactions amplify the nonlinear response associated with the Lorentz field, rendering bistability much easier to observe. It confirms experimentally that cooperative nonlinearities can induce hysteretic behavior in crystals *without* a cavity. Bistability from this mechanism can be expected to occur also in avalanche systems which decay by runaway cross relaxation, and it has a variety of potential applications in all-optical switching for communications and optical computing. Our results are most pertinent to stationary atoms in solids and suggest that bistability is expected to be most pronounced in compounds containing well-isolated strongly coupled ion arrangements such as dimers. Furthermore, these results have broader implications for selected transitions in vapors which induce quasiresonant collisional interactions. Similar effects may occur in high density optical traps below the Doppler cooling limit when internuclear separation does not change appreciably during an excited-state lifetime. Finally, these results suggest new extensions of theories of the local field[18] in dense atomic systems.

[1] M. P. Hehlen, H. U. Güdel, J. Rai, S. Rai, and S. C. Rand, Phys. Rev. Lett. **73**, 1103 (1994).
[2] C. M. Bowden and C. C. Sung, Phys. Rev. A **19**, 2392 (1979).
[3] F. A. Hopf, C. M. Bowden, and W. Louisell, Phys. Rev. A **29**, 2591 (1984).
[4] F. A. Hopf and C. M. Bowden, Phys. Rev. A **32**, 268 (1985).
[5] Y. Ben-Aryeh, C. M. Bowden, and J. C. Englund, Phys. Rev. A **34**, 3917 (1986).
[6] M. E. Crenshaw, M. Scalora, and C. M. Bowden, Phys. Rev. Lett. **68**, 911 (1992).
[7] H. U. Güdel, A. Furrer, and H. Blank, Inorg. Chem. **29**, 4081 (1990).
[8] M. P. Hehlen and H. U. Güdel, J. Chem. Phys. **98**, 1768 (1993).
[9] A. C. Tam, T. Yabuzaki, S. M. Curry, M. Hou, and W. Happer, Phys. Rev. A **17**, 1862 (1978).
[10] A. Lenef, D. Kreysar, K. Obermyer, and S. C. Rand, Phys. Rev. A **51**, 1731 (1995).
[11] M. Allegrini, C. Gabbanini, and L. Moi, J. Phys. Paris, Colloq. **46**, C1-61 (1985).
[12] J. S. Chivian, W. E. Case, and D. D. Eden, Appl. Phys. Lett. **35**, 124 (1979).
[13] M. P. Hehlen, K. Krämer, H. U. Güdel, R. A. McFarlane, and R. N. Schwartz, Phys. Rev. B **49**, 12475 (1994).

[14] H. A. Lorentz, *The Theory of Electrons*, 2nd ed. (Dover, New York, 1952), Sections 117–136 and note 54.

[15] R. G. Brewer, *Coherent Optical Spectroscopy*, in *Frontiers in Laser Spectroscopy*, edited by R. Balian, S. Haroche, and S. Liberman, Vol. 1 (North-Holland, Amsterdam, 1977), pp. 341–398.

[16] C. M. Bowden and J. P. Dowling, Phys. Rev. A **47**, 1247 (1993).

[17] M. Sargent, M. O. Scully, and W. E. Lamb, *Laser Physics* (Addison-Wesley, Reading, 1974), pp. 84–87.

[18] J. Van Kranendonk and J. E. Sipe, in *Progress in Optics XV*, edited by E. Wolf (North-Holland, Amsterdam, 1977), p. 245; F. Hynne and R. K. Bullough, Philos. Trans., R. Soc. London, Ser A **312**, 251 (1984); **321**, 305 (1987); **330**, 253 (1990).

[19] U. Oetliker, M. J. Riley, P. S. May, and H. U. Güdel, J. Lumin. **53**, 553 (1992).

[20] H. Ni and S. C. Rand, Opt. Lett. **16**, 1425 (1991).

[21] D. L. Dexter, J. Chem. Phys. **21**, 836 (1953).

[22] H. S. Carslaw and J. C. Jäger, *Conduction of Heat in Solids* (Oxford University, London, 1948).

[23] G. Meyer, Prog. Solid State Chem. **14**, 141 (1982).

[24] A. Dönni, A. Furrer, and H. U. Güdel, J. Solid State Chem. **81**, 278 (1989).

[25] E. Nakazawa and S. Shionoya, Phys. Rev. Lett. **25**, 1710 (1970).

[26] M. P. Hehlen, G. Frei, and H. U. Güdel, Phys. Rev. B **50**, 16264 (1994).